Proceedings of the
Annual Stability Conference
Structural Stability Research Council
Toronto, Canada, March 25-28, 2014

Modeling of moment connections for structural fire analyses

M. Seif [1], T. McAllister [2], J. Main [3], W. Luecke [4]

Abstract
Performance-based methodologies to evaluate the fire performance of structures are needed to move beyond the prescriptive procedures presently in use, which cannot be used to determine actual structural performance in fire. Analytical methods are needed for simulating the performance of structural systems, including connections, subject to realistic fire effects. Framing connections may be subject to large unanticipated deformations and loads during fire events, and connection failure may lead to other failures or local collapse. This paper presents the development of detailed finite element models of typical moment connections for steel framed structures. These detailed models incorporate temperature-dependent material models that have been calibrated against available test data from tensile coupons, including the modeling of necking behavior and fracture. The detailed connection models are loaded to failure to identify the applicable failure mechanisms. Connection performance at ambient and elevated temperatures is evaluated, and dominant failure modes are identified.

1. Introduction

There is a lack of tools for modeling the response of structural system response, including connections, to realistic, uncontrolled fires. Fire protection of steel structures is usually provided through prescriptive requirements based on the standard fire test (ASTM 2011) which has changed little since it was introduced in 1917. Such tests typically characterize heat transmission through elements and subsystems, but do not provide information about structural performance in real fire. A fuller understanding of the problem will lead to the development of analytical tools and design standards that explicitly consider realistic fire loading for both the design of new buildings and assessment and retrofit of existing ones. Development of design tools for evaluating fire effects usually requires detailed finite element (FE) analyses that consider all failure modes, including local buckling, at elevated temperatures.

[1] Research Structural Engineer, National Institute of Standards and Technology (NIST), Gaithersburg, MD, mina.seif@nist.gov
[2] Research Structural Engineer, National Institute of Standards and Technology (NIST), Gaithersburg, MD, therese.mcallister@nist.gov
[3] Research Structural Engineer, National Institute of Standards and Technology (NIST), Gaithersburg, MD, joseph.main@nist.gov
[4] Materials Research Engineer, National Institute of Standards and Technology (NIST), Gaithersburg, MD, william.luecke@nist.gov

During exposure to fire, large axial compressive and/or tensile forces may develop in floor beams and their connections. A number of researchers have studied the effects of fire on connections, though most of the literature addresses shear connections and semi-rigid connections. Sarraj et al. (2007) developed detailed solid element models for shear tab connections with bolts to evaluate bolt shear and bearing behavior. Yu et al. (2009) performed an experimental investigation of the behavior of shear tab connections subjected to vertical shear and tensile forces at elevated temperatures and measured the moment-rotation capacity of the shear tab connections. Seif et al. (2013) discussed failure modes of shear-tab connections at elevated temperatures. Yang et al. (2009) conducted experimental tests of welded moment connections where connections and members immediately adjacent to the connection were heated to 550 °C to 650 °C and then loaded to failure under an applied moment (top flange in tension and bottom flange in compression). Yielding, necking, fracture, bolt elongation (shear), and local buckling were observed, and a reduction of member stiffness to 25% of ambient values was reported. Quiel and Garlock (2010) conducted detailed finite element analyses of shear and moment connections for 2D and 3D building frames. Their results indicate that thermal gradients can produce significant changes in the deflection mechanics and plastic *P-M* limit-state behavior.

This paper presents a study employing FE analysis with geometric and material nonlinearities, using solid elements to model the failure modes of typical steel connections in response to elevated temperatures. Recently developed temperature-dependent material models for different types of steels used in connections are implemented. FE analyses of coupon models are performed to verify the implementation of these material models. Results are presented that illustrate the detailed modeling of the connection and the failure modes under varying load and temperature conditions. These analyses will be used to formulate reduced connection models for FE analyses of structural systems at ambient and elevated temperatures.

2. Prototype Building Designs

As described in Lew et al. (2013), NIST worked with a panel of practicing structural engineers across the U.S. to develop a number of prototype steel-frame building designs for use in assessing the robustness of structural systems. The buildings were designed according to the American Society of Civil Engineers 7-02 standard (ASCE 2002) and its referenced material design standards, including the American Institute of Steel Construction (AISC) "Load and Resistance Factor Design Specification for Structural Steel Buildings" (AISC 1999) and the AISC "Seismic Provisions for Structural Steel Buildings" (AISC 2002). These prototype buildings are considered representative of typical construction, and a moment connection from one of the prototype buildings, shown in Fig. 1, was selected for analysis in this study.

The moment connection shown in Fig. 1 is a welded unreinforced flange, bolted web (WUF-B) connection, which is one of the prequalified steel connections listed in FEMA 350 (FEMA 2000). The WUF-B connection in Fig. 1 is taken from the second-floor level of a seismically designed intermediate moment frame (IMF) in a 10-story prototype building designed for Seismic Design Category C. The number and size of the ASTM A490 bolts varied for the WUF-B connections within the moment frames, as did the thickness and height of the shear tabs. ASTM A992 structural steel (F_y = 344.8 MPa) was used in all beams and columns. ASTM A36 steel (F_y = 248.2 MPa) was used for the shear tabs and continuity plates at the beam-column connections.

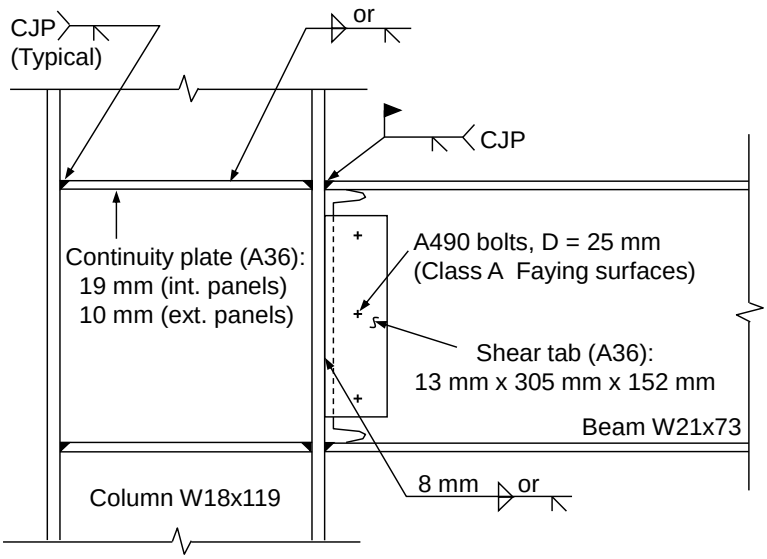

Figure 1. Details of WUF-B moment connection.

3. Connection FE Modeling

Detailed nonlinear FE analyses were conducted to simulate the failure modes of moment connections under elevated temperatures. In each analysis, the connection was subjected to a monotonically increasing axial displacement, either tensile or compressive. Analyses were performed using explicit time integration in LS-DYNA (LSTC 2012), and the prescribed displacements were applied gradually to ensure that dynamic effects were negligible (i.e., to ensure quasi-static loading conditions). Both compressive and tensile loading conditions are of interest because they represent the types of loading imposed on connections in the heating and cooling phases of a fire, respectively.

While the displacements imposed on a connection in a realistic fire depend on the temperature distribution within the structural elements and the thermal restraint imposed by the structural configuration, the simple loading protocol considered (see Fig. 2) enabled investigation of the behavior, failure modes, and ultimate capacities of the connections at different temperatures. Analyses under prescribed displacements were performed at four temperatures (20 °C, 400 °C, 500 °C, and 600 °C), with the temperature in each analysis being uniform and constant. With constant temperature throughout each analysis (i.e., temperatures were not ramped up from the ambient temperature), no stresses due to restraint of thermal expansion were present in the analyses.

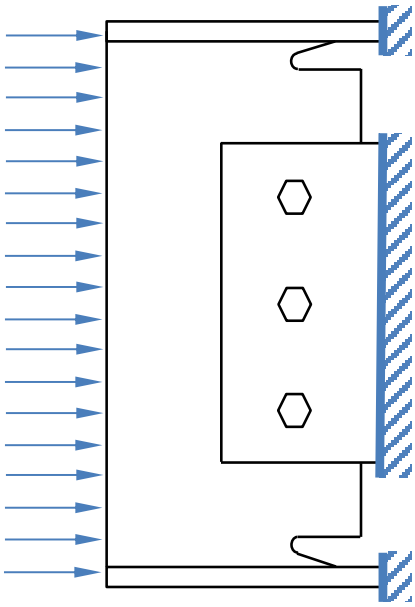

Figure 2. Schematic view of compressive axial displacements imposed on a WUF-B connection.

The WUF-B connection shown in Fig. 1 was modeled using finely meshed three-dimensional solid elements for the beam, bolts, and shear tab, as shown in Figure 3. Fully integrated eight-node solid elements were used. A typical element size of 0.12 in (3 mm) was used for the beam and the shear tab. A finer mesh with a typical element size of 0.06 in (1.5 mm) was used for the bolts. Contact was defined between the bolts, shear tab, and beam web to model the transfer of forces through the bolted connection, including friction, with a value of 0.3 assumed for both the static and dynamic coefficients of friction. No pre-tension in the bolts was considered in the analyses. All degrees of freedom were restrained for nodes on the welded ends of the shear tab and the beam flanges.

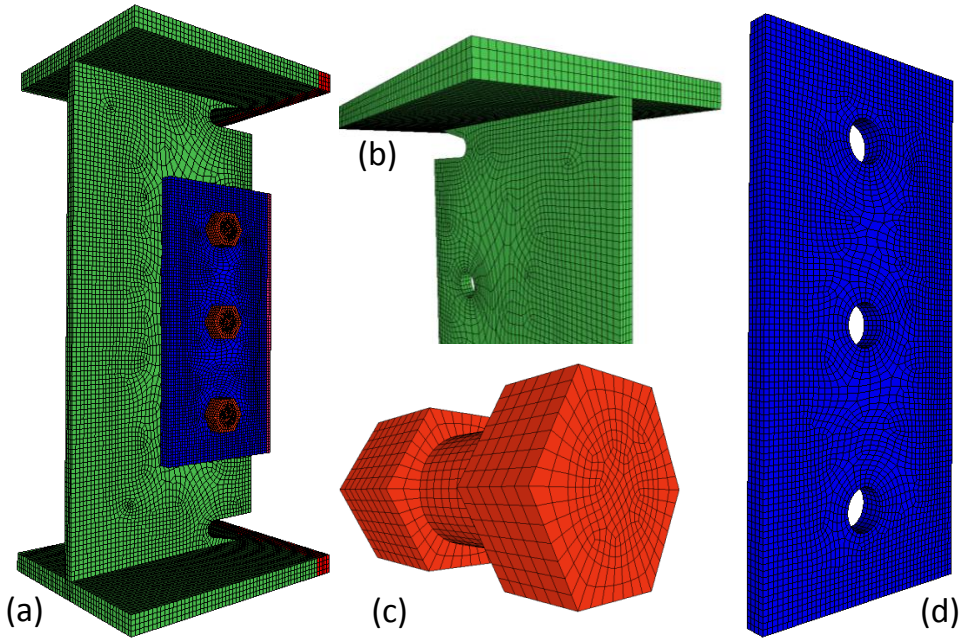

Figure 3. Detailed model of the WUF-B connection: (a) full model, (b) beam, (c) bolt, and (d) shear tab.

The temperature-dependent material models used for finite element (FE) analysis of shear and moment connections at elevated temperatures are discussed in the following section. ASTM A572 Grade 50 steel, with an ambient-temperature yield strength of F_{y0} = 50 ksi (345 MPa), is used for the beam and column, and ASTM A36 steel, with F_{y0} = 36 ksi (250 MPa), is used for the shear tab. ASTM A490 bolts, with F_{y0} = 130 ksi (896 MPa), are used for the WUF-B connection (see Fig. 1 for connection details).

4. Temperature-Dependent Material Modeling

A key issue in evaluating the response of structural systems to fire effects is the representation of material behavior at elevated temperatures. In addition to stress-strain behavior, modeling of fracture is required to capture failure modes such as tear out in connection plates and bolt shear. The use of explicit finite element software packages allows for modeling of sequential failures, including fracture. Fracture can be simulated using element erosion, in which elements are removed from the analysis when specified failure criteria are satisfied. However, the basis for determining and implementing material failure criteria at elevated temperatures is not well-established in the literature. This section presents a finite element material modeling methodology for structural steels at elevated temperatures including erosion-based modeling of fracture. A recently developed temperature-dependent material model for structural steels is combined with a plastic strain-based failure criterion for element erosion. Using finite element models of tensile coupons, this failure criterion is calibrated against experimental data on elongation at fracture, and the influence of temperature and mesh size on the failure criterion is investigated.

Luecke et al. (2013) developed an empirical model that provides temperature dependent material models for any structural steel. The model is based on experiments conducted at the National Institute of Standards and Technology (NIST) and published data from numerous experiments reported in the literature. The model accounts for the change in yield strength and post-yield strain hardening with temperature. However, the model does not account for creep effects. Equations for true stress and true strain, shown below, are required to define material models in LS-DYNA analyses. However, as is discussed subsequently, detailed finite element models of tensile coupons are used to obtain engineering stress-strain curves for comparison with experimental measurements, particularly regarding the post-ultimate behavior, including necking and fracture.

Experimental data to support temperature-dependent material properties for structural bolts are more limited than for structural steel, particularly data regarding the temperature-dependence of deformations or elongations at fracture. Much of the available experimental data for bolt shear tests is influenced by deformation of the shear loading assembly, making it difficult to isolate the bolt performance. Given these limitations, an interim approach for modeling the temperature-dependent nonlinear material behavior and fracture of bolts is described below.

4.1 Structural Steel

For structural steel (beams, columns, and shear tabs), the temperature-dependence of the yield strength F_y is expressed as:

$$F_y(T) = F_{y0} \cdot \left[r_5 + (1 - r_5) \cdot \exp\left(-\frac{1}{2}\left(\frac{\Delta T}{r_3} \right)^{r_1} - \frac{1}{2}\left(\frac{\Delta T}{r_4} \right)^{r_2} \right) \right] \tag{1}$$

where F_{y0} is the yield strength at ambient temperature, ΔT (in °C) is the increase in temperature above the ambient temperature, and r_1 through r_5 are coefficients depending on the type of steel. For rolled structural steel, r_1 = 7.514, r_2 = 1.000, r_3 = 588 °C, r_4 = 676 °C, and r_5=0.090.

The elastic modulus E (in GPa) is expressed a function of the temperature T (in °C) as follows:

$$E(T) = E_0 \cdot \left[\exp\left(-\frac{1}{2}\left(\frac{\Delta T}{e_3} \right)^{e_1} - \frac{1}{2}\left(\frac{\Delta T}{e_4} \right)^{e_2} \right) \right] \tag{2}$$

where E_0 = 206 GPa (2987 ksi) is the value at ambient temperature, and e_1 through e_4 are coefficients depending on the type of steel. For rolled structural steel, e_1 = 3.768, e_2 = 1.000, e_3 = 639 °C, and e_4=1650 °C.

The true stress σ_{true} is expressed as a function of true strain ε_{true} as follows:

$$\sigma_{true} = \begin{cases} E(T)\,\varepsilon_{true} & \text{for } \varepsilon_{true} < \dfrac{F_y(T)}{E(T)} \\ \left(F_y(T) + \left(1006 - 0.759 F_{y0}\right) \exp\left(-\left(\dfrac{T}{540} \right)^{7.82} \right) \left(\varepsilon_{true} - \dfrac{F_y(T)}{E(T)} \right)^{0.503} \right) & \text{for } \varepsilon_{true} \geq \dfrac{F_y(T)}{E(T)} \end{cases} \tag{3}$$

where it is noted that E and F_y depend on temperature according to Eqs. (1) and (2). Fig. 4 shows the true stress-strain curves for the A572 steel, generated using this temperature-dependent material model. The point corresponding to the ultimate engineering stress (also referred to as the tensile strength) for each temperature is indicated by a red dot, and the true stress-strain curves are extended linearly beyond this point, as discussed subsequently.

Eq. (3) was calibrated to match available experimental data up to the tensile strength, and special care is needed in modeling the post-ultimate material behavior, including necking and fracture. Seif et al. (2013) developed an approach for modeling the post-ultimate behavior of structural steel at elevated temperatures, by using element erosion to represent fracture. The onset of erosion was calibrated to match available experimental data of fracture in coupons at elevated temperatures. Since the simulation of post-ultimate necking and fracture depends on the model mesh size, the coupon models had the same mesh size as the connection model for the calibration procedure. The calibration is invalid if the mesh sizes between the coupon and the model are different. The stress-strain relationship computed from Eq. 3 was used up to the ultimate engineering stress, after which the post-ultimate stress associated with necking and fracture was modeled with a tangential extension from the ultimate stress.

The failure criterion used for element erosion is based on the effective plastic strain, a scalar measure of plastic strain that incorporates its various tensor components. Element erosion is activated when the effective plastic strain in any element (i.e., the local plastic strain in a section or component) exceeds a specified critical value, called the erosion strain ε_{er}. Analyses of detailed, three-dimensional solid element models tensile coupons were conducted to calibrate the erosion strain values against available experimental data on elongation of tensile coupons, including data for ASTM A992 steel from Hu and Morovat (2009) and data for ASTM A572 Grade 50 steel from Luecke (2005). Temperature-dependent values of the erosion strain were used in order to achieve the best agreement with the experimental data.

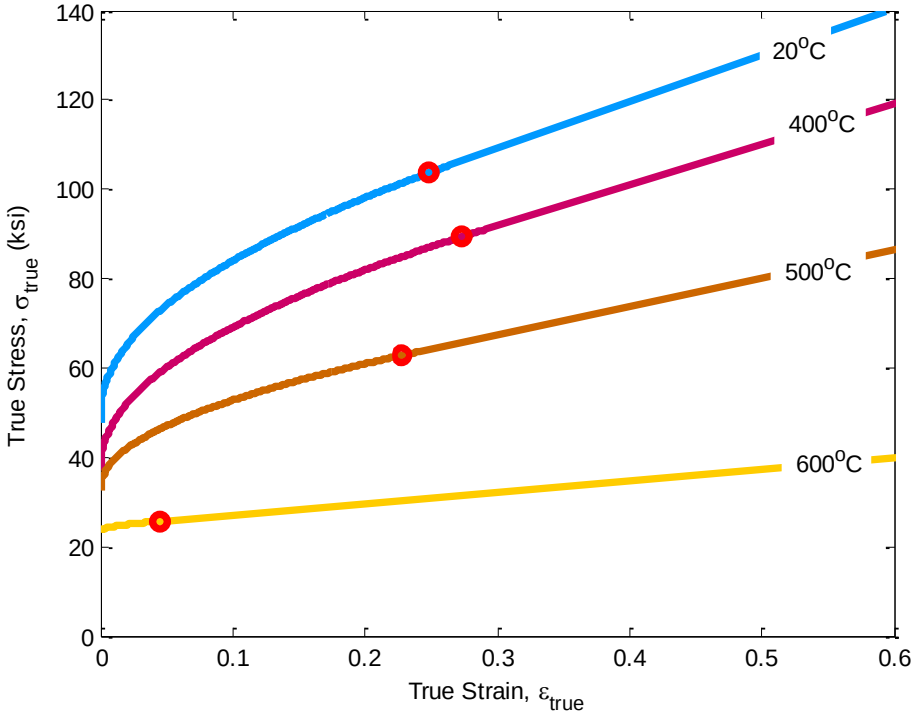

Figure 4. True stress-strain curves for A572 steel, generated with Luecke et al. (2013) temperature-dependent material model (1 ksi = 6.895 MPa).

As the value of ε_{er} increases, the computed engineering strain at fracture also increases. For instance, at 400 °C, when $\varepsilon_{er,}$ increases from 0.70 to 0.90, the engineering strain at fracture, $\varepsilon_{eng,f}$, increases by about 10% from 0.45 to 0.50. To determine the appropriate value of erosion strain at each temperature, the erosion strain was adjusted until the resulting engineering strain at fracture matched a target value determined from the available experimental data. The target value of the engineering strain at fracture was selected as the mean value of experimental data at each temperature of interest (20 °C, 400 °C, 500 °C, and 600 °C), and is plotted along with the experimental data in Fig. 5.

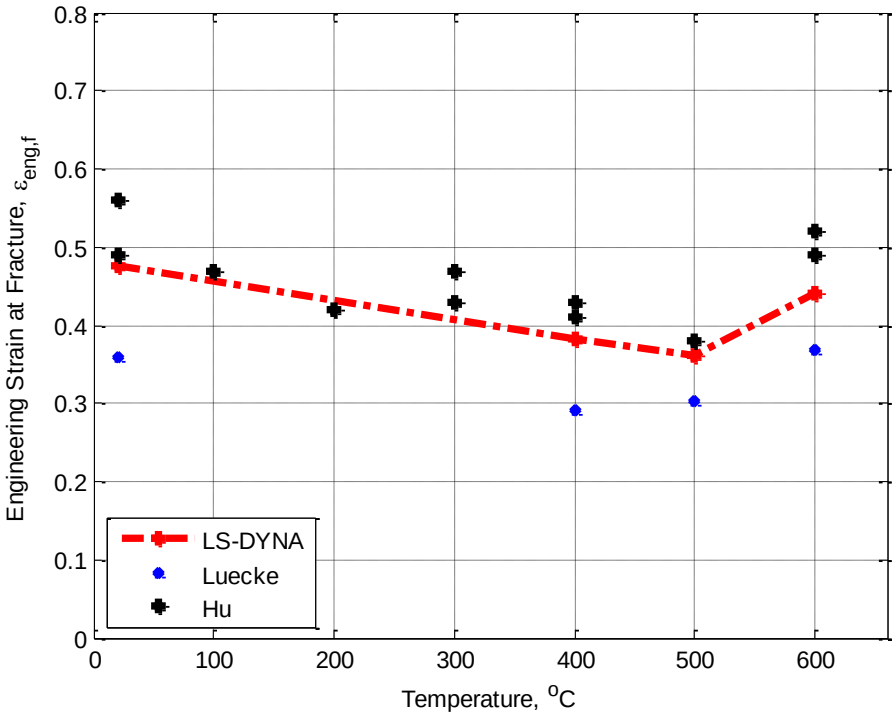

Figure 5. Target values of engineering strain at fracture determined from experimental data.

The values of erosion strain ε_{er} in the FE model that matched the target values of engineering strain at fracture shown in Fig. 5 for Grade 50 structural steels are listed in Table 1. Note that beyond 500 °C, the erosion strain greatly increased due to increased plasticity at elevated temperatures. Fig. 6 shows engineering stress-strain curves obtained from FE analysis of tensile coupons for the engineering strain at fracture values shown in Fig. 5 at temperatures of 20 °C, 400 °C, 500 °C, and 600 °C. Due to the calibration procedure described above, the engineering strain values at fracture in Fig. 6 closely match the target values in Fig. 5. Note that due to the lack of experimental data in the literature regarding the effect of elevated temperatures on the strain at fracture of mild steel, A36 (of which the shear tabs are typically constructed), the values of ε_{er} were assumed to be equal to those of the A572 steel for the purpose of the analysis. This assumption did not affect the results, as no fracture occurred in the shear tab.

Table 1. Engineering and erosion strain values at fracture for structural steel.

Temperature (°C)	Engineering Strain at Fracture	Erosion Strain at Fracture
20	0.47	0.70
400	0.38	0.35
500	0.35	0.40
600	0.46	1.40

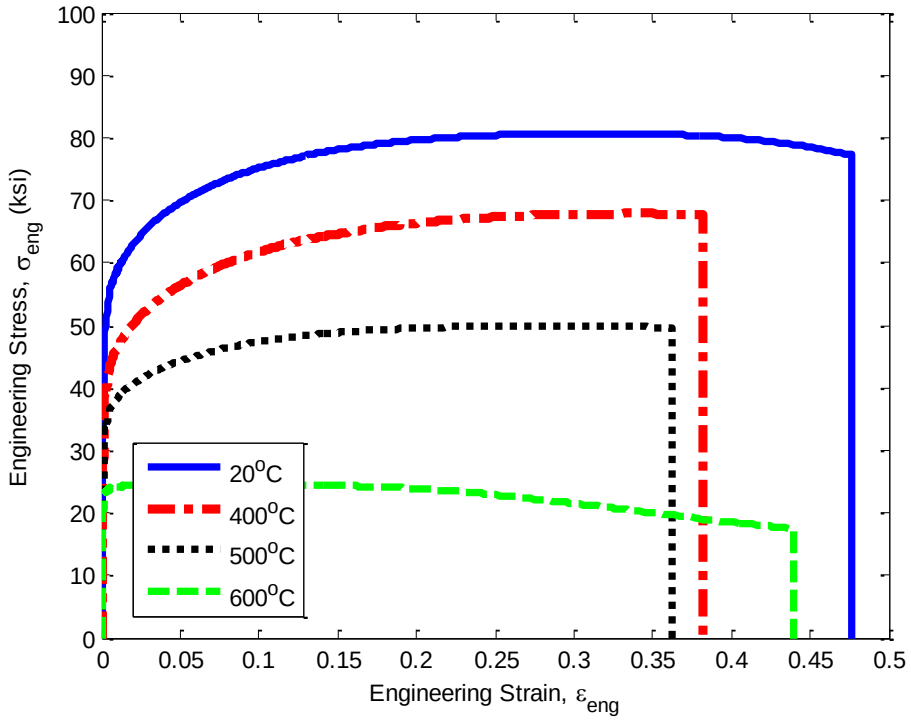

Figure 6. Target values of engineering strain at fracture determined from experimental data.

4.2 Bolts

For high-strength bolts (A325 and A490), the temperature-dependence of the yield strength F_y is calculated from Eq. (1), with $r_1 = 4.967$, $r_2 = 1.000$, $r_3 = 456$ °C, $r_4 = 2040$ °C, and r_5=0.000. Compared to rolled steel, bolts sustain their F_y value with the increase of temperature up till about 400 °C, after which it drops dramatically. Fig. 7 shows the degradation of the normalized yield strength with increasing temperature for ASTM A572 rolled steel and ASTM A325 and A490 bolts. Note that at 400 °C, both rolled steel and bolts sustain about 80 % of their yield capacity. At 600 °C, rolled steel sustains about half of its yield capacity, while bolts lost more than 82% of their yield capacity. The ultimate strength F_u is calculated by using Eq. (1) with the same values of r_1 through r_5 as for the yield strength, but with the ambient-temperature yield strength F_{y0} replaced by the ambient-temperature ultimate strength F_{u0}.

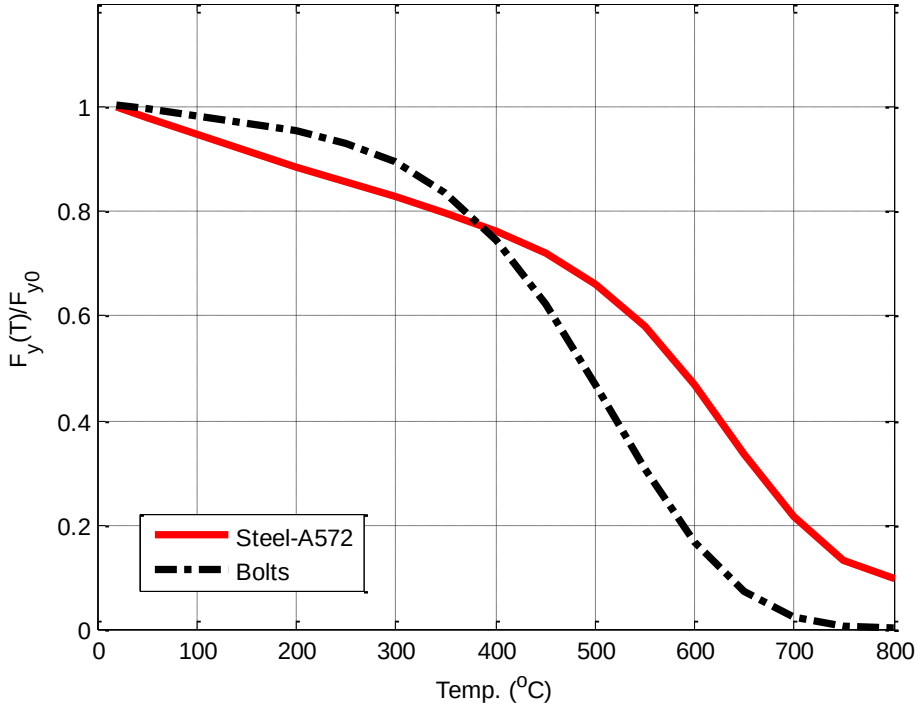

Figure 7. Degradation of normalized yield strength versus the increase in temperature for rolled structural steel and bolts.

The elastic modulus E for bolts is the same as that for rolled steel, calculated from Eq. (2). The stress-strain relationship is not calculated from Eq. (3), but rather a tri-linear relationship as follows:

$$\sigma_{true} = \begin{cases} E(T)\varepsilon_{true}, & \varepsilon_{true} \le \varepsilon_y(T) \\ F_y(T) + \left[F_u(T) - F_y(T)\right]\dfrac{\varepsilon_{true} - \varepsilon_y(T)}{\varepsilon_u(T) - \varepsilon_y(T)}, & \varepsilon_y(T) < \varepsilon_{true} \le \varepsilon_u(T) \\ F_u(T) + 0.08E(T)\left[\varepsilon_{true} - \varepsilon_u(T)\right], & \varepsilon_u(T) < \varepsilon_{true} \end{cases} \quad (4)$$

where $\varepsilon_y(T) = F_y(T)/E(T)$ is the temperature dependent yield strain. The temperature-dependent ultimate strain, $\varepsilon_u(T)$, is assumed to have a value of 0.1 at 20°C and to decrease linearly with temperature to a value of 0.05 at 600 °C. Fig. 8 shows the tri-linear stress-strain relationship of the A325 bolts at 20 °C, 400 °C, 500 °C, and 600 °C. Similar to rolled steel, the failure criterion used for element erosion is based on the effective plastic strain. Element erosion is activated when the effective plastic strain in any element exceeds ε_{er}. The erosion strain is temperature-dependent and based on analyses of detailed, three-dimensional solid-element models of A325 and A490 steel bolts. The values of ε_{er} were calibrated against available experimental data from Kodur at al. (2012). To determine the appropriate value of erosion strain at each temperature, the erosion strain was adjusted until the resulting engineering strain at fracture matched a target value determined from the available experimental data. Values of engineering strain and erosion strain at fracture for the A325 and A490 bolts reported by Kodur et al. are listed in Table 2. A

more detailed discussion of the temperature-dependent models for structural steels at elevated temperatures is provided in Seif et al. (2014).

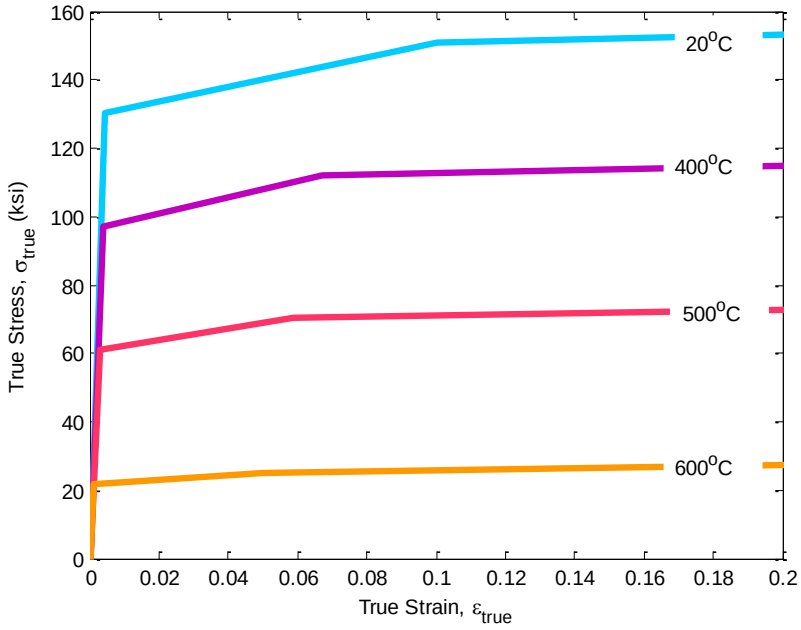

Figure 8 True stress-strain curves for A325 bolts at 400°C (1 ksi = 6.895 MPa).

Table 2. Engineering and erosion strain values at fracture for A325 and A490 bolts.

Temperature (°C)	Engineering Strain at Fracture		Erosion Strain at Fracture	
	A325	A490	A325	A490
20	0.210	0.16	0.50	0.35
400	0.204	0.16	0.55	0.40
500	0.246	0.19	0.75	0.55
600	0.276	0.22	0.75	0.60

5. Results and Discussion

The discussion in this section focuses on the behavior and failure modes of the WUF-B connection subjected to axial loading, as illustrated in Fig. 2. Fig. 10 shows the total axial load versus displacement curves for the WUF-B connection under both tensile and compressive loading at different temperatures. The displacement plotted in Fig. 10 (and in Figs. 11 and 12 subsequently) is the axial displacement imposed at the free end of the beam (the left end in Fig. 2). A uniform axial displacement is imposed for the entire cross section, with out-of-plane displacements unrestrained. Results in Fig. 10 show that, despite differences in failure modes, the overall capacity of the connection did not differ significantly between tensile and compressive loading conditions for each temperature (differences less than 5 %). Results also show that increasing the temperature from 20 °C to 400 °C reduced the capacity of the connection by only about 20 %. However, increasing the temperature from 400 °C to 500 °C reduced the capacity an additional 30 %. By 600 °C the ultimate capacity of the connection has dropped by about 70 %.

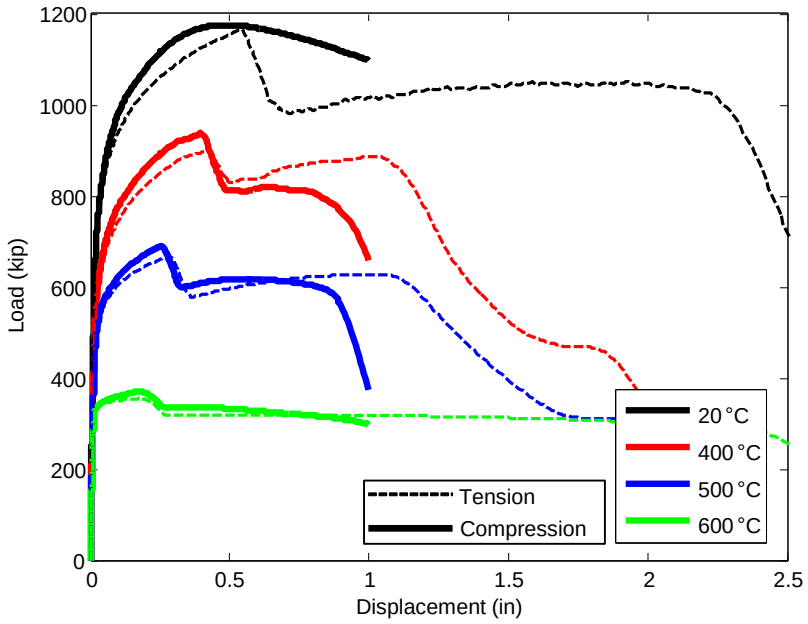

Figure 10 Load-displacement curves for the WUF-B connection at different temperatures (1 kip = 4.448 kN, 1 in = 25.4 mm).

In developing reduced models to capture the connection behavior at elevated temperatures, it is important to consider the contribution of each component of the connection in resisting axial loads. To this end, the total axial force in the WUF-B connection, as shown in Fig. 10, can be decomposed into the axial forces in each of five components of the connection: the two flanges and three bolt rows. The axial force in a single flange can be obtained by summing the reaction forces of all nodes at the welded end of that flange (at the right end in Fig. 2). Fig. 11 shows a resulting plot of the axial force in a single flange of the WUF-B connection against the axial displacement imposed on the free end of the beam. The axial force in each bolt row can be obtained by defining three sets of nodes at the welded end of the shear tab, corresponding to three strips of the shear tab with equal height, each containing a single bolt. Summing the reaction forces of all nodes corresponding to a single strip then gives the force in that bolt row. Fig. 12 shows a resulting plot of the axial force in a single bolt row against the axial displacement imposed on the free end of the beam.

Figs. 11 and 12 (note the different scales on the vertical and horizontal axes) show that the flanges of the WUF-B connection have much greater capacity than the bolts and that they can sustain much greater deformations before fracture. The peak values in the total load-displacement curves in Fig. 10 correspond to the ultimate load in the bolt rows, while the connection continues to sustain substantial load beyond this point through the contribution of the flanges. Fig. 11 shows that at 20 °C, the flange of the WUF-B connection can sustain deformations exceeding 2 in (51 mm). However, this axial deformation at fracture is about twice as large as what was calculated using a previously developed model of this WUF-B connection (Sadek et al. 2013). The differences are believed to be due in large part to the modeling of the k-area of the beam section, where the web thickness increases as it joins the flange. The increased web thickness, which was accounted for by Sadek et al. (2013) but not in the present study, forces plastic deformations into a smaller portion of the flange, thus reducing the deformation at fracture. This issue will be further investigated in subsequent studies.

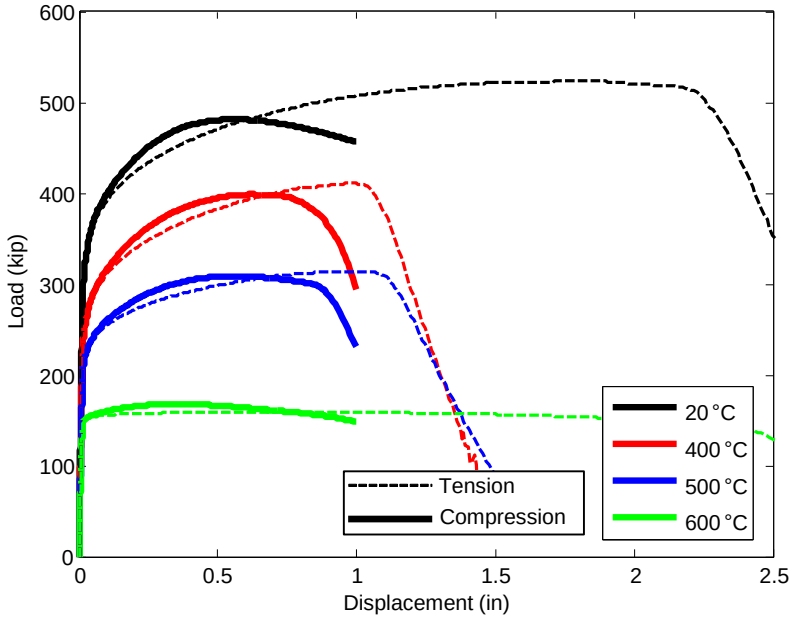

Figure 11 Load-displacement curves for a single flange of the WUF-B connection at different temperatures (1 kip = 4.448 kN, 1 in = 25.4 mm).

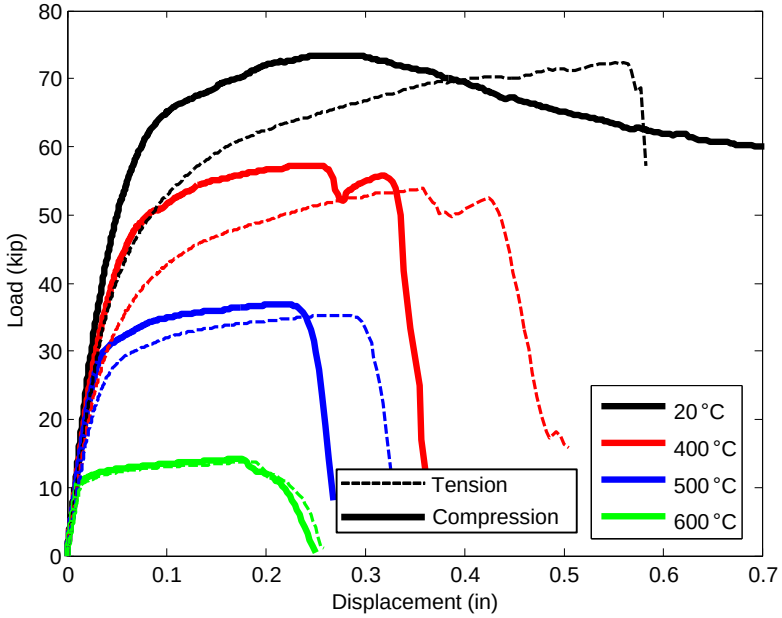

Figure 12 Load-displacement curves for a single bolt row of the WUF-B connection at different temperatures (1 kip = 4.448 kN, 1 in = 25.4 mm).

The failure modes of the WUF-B connection depend on the relative reduction in the yield capacity with the increase in temperature between the rolled steel sections and the bolts. As mentioned in Section 4.2 and shown in Fig. 8, both the A572 steel and the A490 bolts sustain 80% of their yield strength until 400 °C, after which the A490 bolts lose their yield capacity

much faster than the A572 steel. Failure modes have a mix of bolt and beam failure up to 400 °C, but only shear fracture failure modes occurred beyond the 400 °C.

The failure modes under tensile loading conditions can be summarized as follows:

(i) At 20 °C, failure is due to shear fracture of the bolts, followed by fracture of the flanges, as shown in Fig. 14(a),

(ii) At 400 °C, tear-out of the beam web around the bolts is followed by fracture of the flanges, as shown in Fig. 14(b),

(iii) At 500 °C and 600 °C, the failure mode was similar to the 20 °C case.

The failure modes under compressive loading can similarly be summarized as follows:

(i) At 20 °C, failure is due to local buckling of the beam cross-section. The tab also bends along the deformed beam section, and no fracture is observed, as shown in Fig. 15(a),

(ii) At 400 °, 500 °C and 600 °C, failure is due to shear fracture of the bolts, followed by local buckling of the flanges, as shown in Fig. 15(b).

All failure modes of the WUF-B connections at different temperatures under tensile and compressive loading conditions are summarized in Table 1.

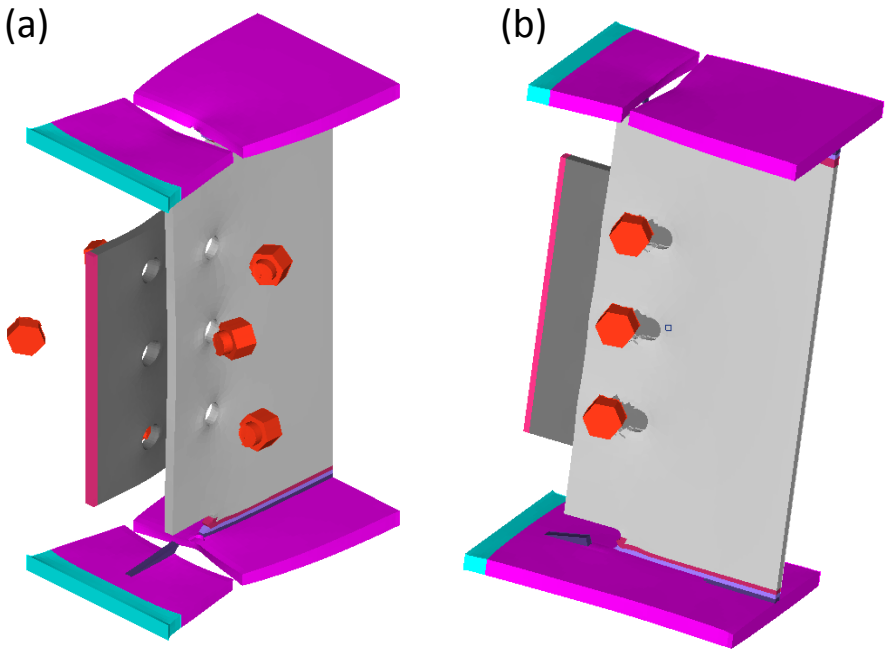

Figure 14 Failure modes of the WUF-B connection in tension: (a) shear fracture in bolts, (b) tear-out in beam web.

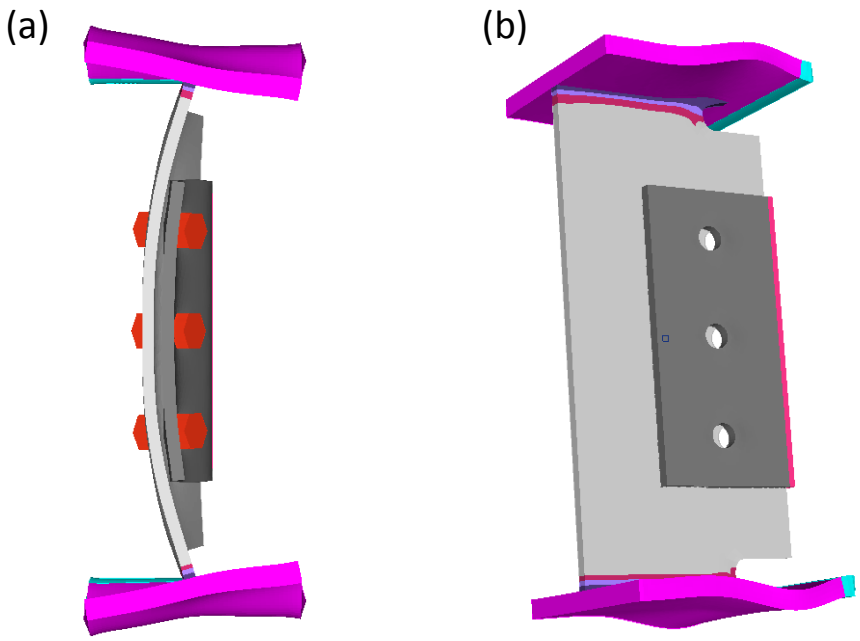

Figure 15 Failure modes of the WUF-B connection in compression: (a) local buckling of beam's cross-section, (b) shear fracture of bolts.

Table 3 Failure modes of the WUF-B connection at different temperatures under tensile and compressive loading conditions.

Temperature	Tensile Failure Mode	Compressive Failure Mode
20 °C	Shear fracture of bolts, followed by fracture of flanges (Fig. 14a).	Beam local buckling, including bending of tab (Fig. 15a).
400 °C	Tear-out of beam web, followed by fracture of flanges (Fig. 14b).	Shear fracture in bolts, followed by local buckling (Fig. 15b).
500 °C	Shear fracture of bolts, followed by fracture of flanges.	Shear fracture in bolts, followed by local buckling.
600 °C	Shear fracture of bolts, followed by fracture flanges.	Shear fracture in bolts, followed by local buckling.

5. Concluding Remarks

This paper presented a detailed finite element analysis approach to determine the performance and failure modes of steel-framed connections subject to elevated temperatures. Finite element models of typical shear and moment connections have been developed that incorporate temperature-dependent material models. Temperature-dependent material models for structural steel and bolts were supplemented with erosion-based failure criteria to simulate fracture. The erosion strains were calibrated by simulating experimental data on elongation of steel coupons at fracture to determine the appropriate local plastic strain value for the model mesh discretization.

The connection models were axially loaded in tension and compression for temperatures of 20 °C, 200 °C, 400 °C, and 600 °C to identify primary failure mechanisms as a function of

temperature, including fracture of bolts, beam and plate elements, local buckling of beam elements, and tear-out failure at bolt holes.

The effect of elevated temperature on the failure modes of WUF-B connections was presented in this paper. Increasing the temperature from 20 °C to 400 °C reduced the overall connection capacity by about 20 % under both tensile and compressive loads. Further increasing the temperature from 400 °C to 500 °C reduced the capacity an additional 30 %. By 600 °C the connection had lost about 70 % of its overall capacity.

Primary failure modes under tensile loading conditions were similar, where shear fracture of the bolts was followed by fracture of the beam flanges, except at 400 °C, where tear-out of the bolts through the beam web occurred rather than bolt fracture. Primary failure modes under compressive loading conditions changed between room temperature and temperatures at or above 400 °C. At 20 °C, the primary failure mode was local buckling of the beam cross section, with no bolt fracture. At 400 °C and above, the failure mode changed to shear fracture of the bolts followed by local buckling of the cross-section.

Disclaimer

Certain commercial software or materials are identified to describe a procedure or concept adequately; such identification is not intended to imply recommendation, endorsement, or implication by the National Institute of Standards and Technology (NIST) that the software or materials are necessarily the best available for the purpose.

References

American Institute of Steel Construction (AISC). (1999). *Load and resistance factor design specifications for structural steel buildings*. Chicago, IL.

American Institute of Steel Construction (AISC). (2002). "Seismic provisions for structural steel buildings." *ANSI/AISC 341-02*, Chicago, IL.

American Society of Civil Engineers (ASCE). (2002). "Minimum design loads for buildings and other structures." *SEI/ASCE 7-02*, Reston, VA.

ASTM (2011), "ASTM Standard E119-11a Standard Test Methods for Fire Tests of Building Construction and Materials", *ASTM International*, West Conshohocken, PA, 2009, DOI: 10.1520/E0119-11A.

Federal Emergency Management Agency (FEMA). (2000). "Recommended seismic design criteria for new steel moment-frame buildings." *FEMA 350*, SAC Joint Venture and FEMA, Washington, D.C.

Hu, G., Morovat, M. A. (2009). "Elevated temperature properties of ASTM A992 steel." ASCE- *Structures Congress Proceedings*, 1067-1076.

Kodur, V., Kand, S., and Khaliq, W. (2012). "Effect of Temperature on Thermal and Mechanical Properties of Steel Bolts." *Journal of Material in Civil Engineering*, 24(6), 765–774.

Lew, H.S., Main, J.A., Robert, S.D., Sadek, F., and Chiarito, V.P. (2013). "Performance of steel moment connections under a column removal scenario. I: Experiments." *Journal of Structural Engineering*, ASCE, 139(1), 98-107.

Livermore Software Technology Corporation (LSTC). (2012), "LS-DYNA Keyword User's Manual." Livermore, CA.

Luecke, W. E., J.D. McColskey, C.N. McCowan, S.W. Banovic, R.J. Fields, T.J. Foecke, T.A. Siewert, F.W. Gayle (2005) "Federal Building and Fire Safety Investigation of the World Trade Center Disaster, Mechanical Properties of Structural Steels." *NIST NCSTAR 1-3D*, National Institute of Standards and Technology, Gaithersburg, MD.

Luecke W., Gross J.L., McColskey J.D. (2013). "High-temperature, tensile, constitutive models for structural steel in fire", AISC *Engineering Journal*, (Submitted).

Quiel, S.E. and M.E.M. Garlock (2010) "Parameters for modeling a high-rise steel building frame subject to fire", *Journal of Structural Fire Engineering*, Vol 1, No. 2, pp 115-134.

Sadek, F., Main, J., Lew, H., and El-Tawil, S. (2013). "Performance of Steel Moment Connections under a Column Removal Scenario. II: Analysis." *Journal of Structural Engineering*., ASCE, 139(1), 108–119.

Sadek, F., Main, J.A., Lew, H.S., Robert, S.D., Chiarito, V.P., El-Tawil, S. (2010). "An Experimental and Computational Study of Steel Moment Connections under a Column Removal Scenario." *NIST Technical Note 1669*, National Institute of Standards and Technology, Gaithersburg, MD.

Sarraj, M., Burgess, I.W., Davison, J.B., Plank, R.J. (2007). "Finite element modeling of steel fin plate connections in fire", *fire Safety Journal*, Vol 42, pp 408-415.

Seif, M., McAllister, T. (2013). "Performance of steel shear tab connections at elevated temperatures." *Proceedings of Structural Stability Research Council Annual Stability Conference*, SSRC 2013, p. 123-135.

Seif, M.S., McAllister, T.P., Main, J.A., Luecke, W. (2014) "Finite element modeling of structural steel component failure at elevated temperatures." *Engineering Structures*. (in review).

Yang, K.C., Chen, S.J., Ho, M.C. (2009) "Behavior of beam-to-column moment connections under fire load" *Journal of Constructional Steel Research*, 65(7),, 1520-1527.

Yu, H., Burgess, I.W., Davison, J.B., Plank, R.J. (2009). "Experimental investigation of the behavior of fin plate connections in fire", *Journal of Constructional Steel Research*, Vol 65, pp 723-736.